Structure and carbonate orientation of vaterite (CaCO₃)

Jianwei Wang* and Udo Becker

Department of Geological Sciences, University of Michigan, Ann Arbor, Michigan 48109, U.S.A.

Abstract

First-principles calculations and molecular-dynamics simulations are employed in this study to further our understanding of the crystal structure and orientational order of carbonate ions in vaterite, which is the least stable polymorph of calcium carbonate. The structural details of vaterite have been controversial but they are prerequisite for investigating and understanding the processes involving vaterite crystal nucleation, growth, and stabilization at a molecular level. The first-principles calculations, using density functional theory with the plane-wave pseudopotential method, are carried out to calculate relative thermodynamic stabilities of proposed structures. Molecular-dynamics simulations with classical empirical potentials, larger computational cells, and fully flexible models at different temperatures are performed to investigate the orientation and order-disorder of the carbonate ions. The results show that the previously accepted structure with disordered CO_3 ions, which are randomly distributed over three orientations parallel to the c axis, is only metastable. By applying a temperature annealing technique to the molecular dynamics simulations, a more stable structure with fully ordered carbonate ions is found that has a hexagonal superstructure. The space group of this newly derived vaterite structure is $P6_522$ (no. 179) with $Z = 18$ and cell dimensions of $\sqrt{3}$ times in a, and 3 times in c of the previous suggested disordered structure. Comparison of experimental observations of X-ray diffraction patterns, enthalpies of transformation to calcite, and volume change by heat treatment with our theoretical calculations indicates that freshly made vaterite is often carbonate-disordered and metastable and can fully or partially transform to a carbonate-ordered structure by aging and heating.

Keywords: Vaterite, crystal structure, order-disorder, quantum mechanical calculations, XRD data, thermodynamics

Introduction

Calcium carbonates occur widely in nature and are the major minerals in many sedimentological environments. They play an important role in biological functions and processes (Heywood 1994; Mann 2001; Skinner 2005; Rodriguez-Navarro et al. 2007), and they are valuable in many industrial applications, such as paper, rubber, plastics, and paint production (Xiang et al. 2006). Vaterite is thermodynamically stable with respect to amorphous calcium carbonate, but metastable with respect to the other two crystalline polymorphs, aragonite, and calcite. Therefore, vaterite is a rare mineral in geologic settings, though it may be an important precursor in several carbonate-forming processes. Its natural occurrence is often associated with biogenic activities (Ariani et al. 1993; Falini et al. 1998, 2005; Kanakis et al. 2001; Mann 2001), as in pancreatic stone or clogging in human heart valves (Falini et al. 1998; Kanakis et al. 2001), hard tissues of fish otoliths (Falini et al. 2005), and crustacean statoliths (Ariani et al. 1993). In vitro, vaterite can be easily synthesized (Plummer and Busenberg 1982; Shen et al. 2006). At ambient conditions, mixing of calcium chloride and sodium carbonate salt solutions leads first to the deposition of an amorphous calcium carbonate phase that, within minutes, transforms to vaterite. If vaterite stays in contact with the solution, within one day, it transforms to calcite, the most stable polymorph. If kept dry, such an abiogenic

vaterite is stable at temperatures up to 670 K (Turnbull 1973). Although less common than the other polymorphs, vaterite and its initial nucleation, growth, and stabilization offer an opportunity to study the mechanism of biomineralization and also to understand crystal nucleation and growth in general (Falini et al. 1998; Champ et al. 2000). However, its crystal structure, the basis for such growth and nucleation studies, is still controversial and not well understood (Medeiros et al. 2007). Thus, before major progress can be made on understanding processes involving the formation and stabilization of vaterite at the atomic level, details of its crystal structure need to be resolved.

Vaterite has the same chemical composition as calcite (rhombohedral) and aragonite (orthorhombic), but with a different crystal structure in terms of symmetry, orientation of CO_3 ions, and coordination environment of Ca ions. There is general agreement that the carbonate planes are parallel to the c axis, which is consistent with its optical properties such as uniaxial positive interference figures with $n_\omega = 1.55$ and $n_\varepsilon = 1.65$ (Kamhi 1963), and that the calcium atoms are in eightfold coordination with oxygen atoms. In contrast, the CO_3 ions in calcite and aragonite are perpendicular to the c-axis, and the calcium atoms have sixfold coordination in calcite and ninefold in aragonite (Kamhi 1963; Villiers 1971; Markgraf and Reeder 1985). For vaterite, its symmetry and space group, dimensions of the unit cell, and orientation and site symmetry of the CO_3 ions are controversial. Meyer (1959) was the first to hypothesize a vaterite crystal structure derived from single-crystal X-ray diffraction experiments

and he reported an orthorhombic unit cell with a space group *Pbnm* and *Z* = 4 (Fig. 1a). In this structure model, all sites are fully occupied, which is not consistent with apparent disordering of oxygen sites originated from multiple carbonate orientations in the structure. Kamhi (1963) found a structure with hexagonal symmetry and space group $P6_3/mmc$ using the same XRD technique (Fig. 1b). There is only one unique carbonate in the unit cell, and each atom of the CO_3 ion is disordered with a partial occupancy of 1/3, which accounts for considerable disorder. Based on numerous diffraction streaks parallel to the *c* direction in the X-ray diffraction pattern (Kamhi 1963), a superstructure with a unit cell rotation of 30° and $a = \sqrt{3} \cdot a'$, $c = 2*c'$, and *Z* = 12 was suggested, apparently owing to partial ordering of the carbonate ions in the vaterite sample. However, details of the superstructure such as symmetry and atomic positions were not provided. Meyer (1969) later provided a structure mainly consistent with Kamhi's (1963) structure, which has the same space group but different carbonate site symmetry. Meyer (1969) also noticed diffuse streaks and satellite reflections in the diffraction pattern and argued that there is possible stacking disorder of single layers of trigonal symmetry related by glide reflections and screw axes along *c*. Again, no details of such stacking faults were discussed. Lippmann (1973) developed an idealized structure from the vaterite-type high-temperature phase of $YbBO_3$ (Bradley et al. 1966) with space group $P6_322$. Spectroscopic methods have been applied to resolve the controversy on the vaterite structure and focused on space group and site symmetry. However, the results are inconsistent, often due to impurities in the samples, mode assignments, and differences of group theory analysis. For example, Sato and Matsuda's infrared spectra (Sato and Matsuda 1969) support Kamhi's structure (Kamhi 1963). Behrens et al. (1995) argued that none of the proposed structures, $P6_3/mmc$ or $P6_322$, is consistent with the Raman spectra that indicate the

existence of two distinct symmetric stretching modes for CO_3 ions (Behrens et al. 1995). Anderson's group theory analysis (Anderson 1996) favors both Kamhi's (1963) and Lippmann's (1973) structures. A more recent Raman study (Gabrielli et al. 2000) shows that Meyer's structure (Meyer 1969) is consistent with the Raman spectra. Although there is no consensus on the structure, some features regarding the vaterite crystal structure emerge: (1) the Ca ions are in a hexagonal sublattice and the unit cell of this sublattice is hexagonal; (2) CO_3 ions are parallel to the *c* axis; and (3) there is considerable disordering of CO_3 ions in the structure.

To better understand and ultimately resolve the controversy on the vaterite crystal structure, quantum-mechanical (first-principles) calculations are used in this study to estimate the relative stability of the structures proposed in the literature. Molecular dynamics (MD) simulation with temperature annealing is used to address disordering and to find an ordered superstructure. The molecular modeling reported here also demonstrates the value of combining these two techniques for predicting crystal structures based on calculating the energetics without any free or fitted parameters and for investigating dynamic phenomena by simulating large systems at finite temperatures.

COMPUTATIONAL METHODS

Quantum-mechanics calculations

Quantum-mechanical calculations are performed within the density functional theory (DFT) framework using plane-wave basis sets as implemented in the VASP package (Kresse and Furthmuller 2004). The projector-augmented wave method (PAW) (Blöchl 1994) and exchange-correlation as parameterized by Perdew-Wang 91 (PW91 functionals) (Perdew et al. 1992; Perdew and Wang 1992) are applied in the generalized gradient approximation (Perdew and Wang 1986) (GGA-PAW). The Monkhorst-Pack scheme for integration in the Brillouin zone is adopted and the number of k-points is determined to be large enough in our calculations for good convergence of total energies as a function of k-point density. A k-point

a   **b**
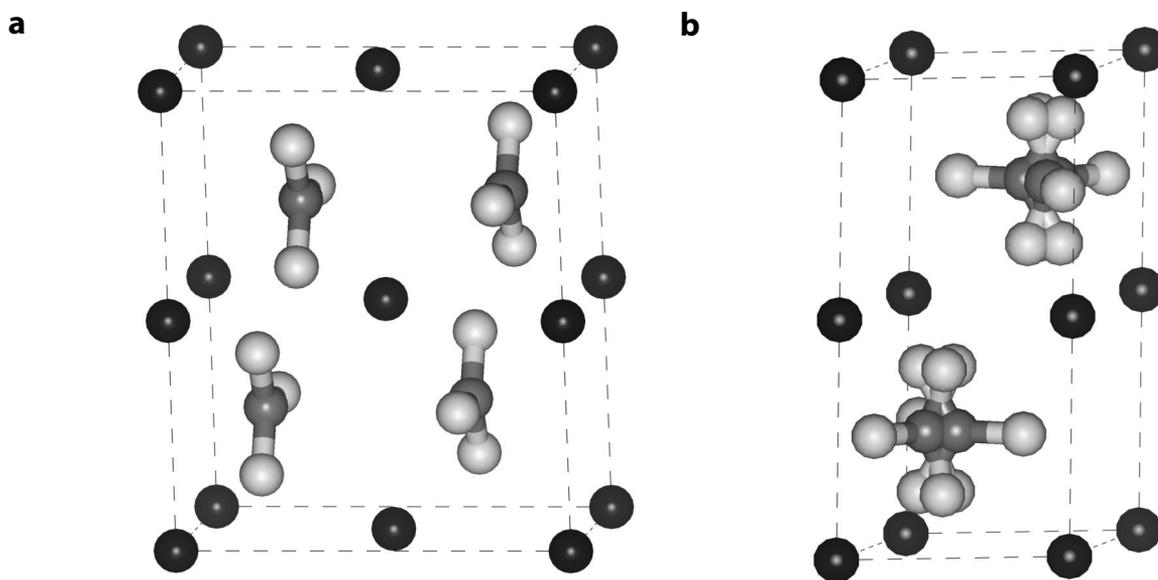
FIGURE 1. Crystal structures of vaterite. Scheme: light gray spheres are oxygen atoms, gray spheres are carbon atoms, and black spheres are calcium atoms. (**a**) Orthorhombic structure with space group *Pbnm* after Meyer (1959). (**b**) Hexagonal structure with space group $P6_3/mmc$ after Kamhi (1963).

mesh of $5 \times 3 \times 3$ is used for the primitive cell to simulate Meyer's orthorhombic structure ($a = 0.413$ nm, $b = 0.715$ nm, and $c = 0.848$ nm) (Meyer 1959) and a $3 \times 3 \times 1$ grid is used for the hexagonal superstructure ($a = b = 0.729$ nm, $c = 2.53$ nm). The energy cutoff for the plane-wave basis set is 520.00 eV or 38.22 Ry in both cases, which was tested for energy convergence. All optimizations allow the volume of the computational cell to relax, and all atoms are free to move. Test cases for the other two polymorphs calcite and aragonite show that the method and computational parameters are adequate to converge the total energy within 0.1 kJ/mol and optimized cell parameters within 1.0%.

Molecular dynamics simulations

Three-dimensional periodic boundary conditions and standard methods and algorithms are used in the MD simulations (Allen and Tildesley 1987). Long-range electrostatic interactions are calculated using Ewald summation based on partial charges at each atom. Lennard-Jones 12-6 potentials with a cutoff method are used for short-range van der Waals interactions. Harmonic bond interactions are used for C-O and O-C-O interactions within the carbonate ion. Non-bonded interactions within the CO$_3$ ion are excluded from the intramolecular interactions. The force field used in our MD simulations is summarized in Table 1 and it is compatible with the CLAYFF force field (Cygan et al. 2004), where an effective force field with partial charges and Lennard-Jones 12-6 potentials is implemented. The Ca force field parameters are taken from the literature (Koneshan et al. 1998; Cygan et al. 2004). The CO$_3$ parameters have been used for carbonate ions in solution (Kalinichev et al. 2001). All MD simulations are performed using NPT ensembles (constant temperature and pressure) with the so-called leap-frog algorithm for the integration of the equations of motion, which is implemented in the GROMACS program (van der Spoel et al. 2005). All atoms in the simulation cell are free to move. The time step for all MD simulations is 1 fs (femtosecond). More details for MD simulation method and applications on minerals are discussed in other publications (de Leeuw and Parker 1998; Cygan 2001; Wang et al. 2001, 2003, 2006).

NPT simulations at isotropic pressure of 1 bar and temperature of 300 K were carried out to estimate unit-cell parameters of calcite and aragonite to validate the models used in our simulations. The computational supercell for calcite was hexagonal and consists of 2160 atoms or 432 CaCO$_3$ units with the dimensions of $2.9928 \times 2.9928 \times 3.4122$ nm and $\gamma = 120°$. The supercell for aragonite was orthogonal and consists of 1200 atoms or 240 CaCO$_3$ units with the dimensions of $2.4807 \times 2.39013 \times 2.29616$ nm. Each system was allowed to equilibrate for 500 ps MD simulation. The equilibrium dynamic trajectory was recorded for statistical analysis at 0.5 ps intervals during an additional 500 ps MD simulation. Statistical averaged unit-cell parameters for calcites are $a = b = 0.4918 \pm 0.0006$ nm and $c = 1.6834 \pm 0.0022$ nm, compared to experimental values of 0.4988 and 1.7061nm (Markgraf and Reeder 1985). Calculated cell parameters for aragonite are $a = 0.4912 \pm 0.0012$ nm, $b = 0.7887 \pm 0.0012$ nm, and $c = 0.5683 \pm 0.0011$ nm, compared to experimental values of 0.49616 nm, 0.79705 nm, and 0.57394 nm (Negro and Ungaretti 1971). The results reproduce all the experimental lattice parameters within 2%. The fluctuations of total energy, temperature, pressure, and cell volume as a function of MD simulation time during the 1 ns MD run for calcite are plotted in Appendix 1.[1]

Temperature-annealing MD simulations (to find disordered and ordered structures in vaterite) were performed at isotropic pressure of 1 bar. The computational supercell consisted of 1080 atoms or 216 CaCO$_3$ units. The supercell is hexagonal with dimensions $2.478 \times 2.478 \times 2.547$ nm. The CO$_3$ orientations were initially arranged to be similar to those of the orthorhombic structure suggested by Meyer (1959). The annealing MD simulation consisted of five annealing cycles at temperatures 0, 50, 300, 500, 1000, and 1500 K. In each annealing cycle, the system temperature started at 0 K and was linearly increased to the highest annealing temperature during the MD run, and then linearly decreased to 0 K again. The total simulation time for the annealing MD was about 7 ns (1 nanosecond = 7 million time steps). At the end of each cycle, the annealed structures were reviewed, and potential energies were calculated. The lattice parameters and potential

energies were therefore calculated at 0 K for comparison with the first-principles calculations. The structure at the end of the 50 K annealing cycle is similar to the orthorhombic structure of Meyer (1959). The structures at the end of each 300, 500, and 1000 K annealing cycles are disordered. The structure at the end of the 1500 K annealing cycle is ordered. This indicates that a temperature of 1500 K is necessary to overcome the activation energy for ordering; however, a much lower temperature would be sufficient to observe ordering, e.g., in days.

Calculations of X-ray diffraction patterns

To compare various model structures of vaterite with experimental results, X-ray diffraction patterns were calculated using the Cerius^2 package (Accelrys 1999), assuming a wavelength of 0.154178 nm (Cu$K\alpha$), Lorentzian peak shapes, and crystal sizes of 50 nm. Indexing of these diffraction patterns was based on the first-principles (GGA-PAW) optimized cell parameters of the ordered superstructure. A module in the Cerius^2 package was used for finding symmetry and to obtain the space group of the MD annealed ordered structure.

RESULTS AND DISCUSSIONS

Structure and energetics

Energetics and unit-cell dimensions of the ordered orthorhombic structure. We use the proposed ordered orthorhombic structure (Meyer 1959) as the starting point (Fig. 1a) and compare how good the agreement is between the experimental structure parameters and our computer-optimized values. The orientation of the CO$_3$ ions in the proposed structure is ordered and parallel to (010), the crystallographic *a-c* plane. All optimized cell parameters based on this structure are systematically larger than experimental values in the *a* dimension and smaller in the *b* dimension, while giving a satisfactory value in the *c* dimension (Table 2). The deviation of calculated cell parameters from experimental data for a given method is approximately as positive for *a* as it is negative for *b* (e.g., GGA-PAW: +11.7 and –10.3%; GGA-PP: +9.7 and –7.1% for *a* and *b*, respectively). The results indicate that the proposed structure over-counts CO$_3$ orientation in the *a* direction, under-counts in the *b* direction, and counts correctly in the *c* direction. In addition to this deficiency regarding cell dimensions of the proposed orthorhombic structure, this ordered structure was also invalidated by the single-crystal X-ray diffraction study by Kamhi (1963), which revealed no evidence for this orthorhombic structure. Orthorhombic symmetry is not consistent with multiple orientations of CO$_3$ ions. Raman spectroscopic results do not support the site symmetry of CO$_3$ of the proposed structure either (Sato and Matsuda 1969; Behrens et al. 1995; Anderson 1996; Gabrielli et al. 2000). Therefore, the

---

[1] Deposit item AM-09-006, Appendix 1. Deposit items are available two ways: For a paper copy contact the Business Office of the Mineralogical Society of America (see inside front cover of recent issue) for price information. For an electronic copy visit the MSA web site at http://www.minsocam.org, go to the American Mineralogist Contents, find the table of contents for the specific volume/issue wanted, and then click on the deposit link there

TABLE 1. Forcefield parameters for MD simulations

	$C^{(6)}$	$C^{(12)}$	Partial charge
Ca	$0.93918 \cdot 10^{-3}$	$0.52704 \cdot 10^{-6}$	+2.000
C	$0.44999 \cdot 10^{-3}$	$0.20995 \cdot 10^{-6}$	+1.123
O	$0.26171 \cdot 10^{-2}$	$0.26331 \cdot 10^{-5}$	–1.041

Notes: Non-bonded interactions:

$$U_{LJ}(r_{ij}) = \frac{C_{ij}^{(12)}}{r_{ij}^{12}} - \frac{C_{ij}^{(6)}}{r_{ij}^{6}}.$$

The cutoff is 0.9 nm. And the combination rules are: $C_{ij}^6 = (C_{ii}^6 \cdot C_{jj}^6)^{1/2}$ and $C_{ij}^{12} = (C_{ii}^{12} \cdot C_{jj}^{12})^{1/2}$.

Interactions within carbonate molecule:

Harmonic bond O-C: $U_B = \frac{1}{2}c_0(b - b_0)^2$ with $b_0 = 0.13$ nm, $c_0 = 644336.0$ kJ/mol/(nm)^2;

Harmonic angle O-C-O: $U_\theta = \frac{1}{2}c_0(\theta - \theta_0)^2$ with $\theta_0 = 120°$, $c_0 = 920.5$ kJ/mol/(rad)^2;

Harmonic improper dihedral C-O$_3$: $U_\psi = \frac{1}{2}c_0(\psi - \psi_0)^2$ with $\psi_0 = 0°$, $c_0 = 2100$ kJ/mol/(rad)^2.

TABLE 2. Cell parameters of Meyer (1959) structure of vaterite (*Pbnm*)

	a (nm) Deviation	*b* (nm) Deviation	*c* (nm) Deviation
GGA-PAW	0.4612 +11.7%	0.6415 –10.3%	0.8473 –0.08%
LDA-PP*	0.4341 +5.1%	0.6432 –10.0%	0.8424 –0.70%
GGA-PP*	0.4531 +9.7%	0.6640 –7.1%	0.8477 –0.04%
Experimental†	0.4130	0.7150	0.8480

* Medeiros et al. 2004.
† Meyer 1959.

crystal structure of vaterite proposed by Meyer (1959) cannot be confirmed by our quantum-mechanical calculations and by the experiments by Kamhi (1963). Thus, partial occupancy and disordering are unavoidable for correctly describing the vaterite structure.

Energetics of the disordered and ordered superstructures. Potential-energy calculations using molecular-modeling methods show that a vaterite structure with CO$_3$ ions distributed over three orientations is more energetically stable than the orthorhombic structure with only one orientation. The structure at the end of the annealing cycle at room temperature (300 K) from our temperature-annealing MD simulation shows that the orientations of CO$_3$ ions are disordered (Fig. 2a) and there are three preferred orientations with an angle of 120° between CO$_3$ planes. However, the structure lacks long-range orientational order. The calculated potential energy per formula from the annealing MD simulation with an annealing temperature of 300 K for this disordered structure is 22.7 kJ/mol more favorable than that of the ordered orthorhombic structure (Table 3). This disordered structure (Fig. 2a), when taking a space average, is consistent with Kamhi's structure (Kamhi 1963) (Fig. 1b), in which each lattice site of the CO$_3$ ion is partially occupied and all atoms of the CO$_3$ ions are randomly distributed among three positions.

However, this fully disordered structure does not account for any degree of long-range ordering in the crystal structure, which was observed in the single-crystal X-ray diffraction patterns, indicated by a small number of weak superstructure reflections (Kamhi 1963). To address possible CO$_3$ orientational ordering, annealing MD cycles were carried out at higher temperature. An ordered superstructure appeared at the end of about 7 ns of simulated annealing with a final annealing temperature of 1500 K. A snapshot of the final structure is shown in Figure 2b. This ordered superstructure is 33.3 kJ/mol more energetically favorable than the ordered orthorhombic structure and 10.6 kJ/mol more favorable than the disordered superstructure (Table 3). The energy contribution from the loss in configurational entropy is relatively small [k$_B$·T·ln(3) ~2.7 kJ/mol] at room temperature if a complete disorder of the CO$_3$ ions over three orientations in the disordered structure is assumed. The GGA-PAW method gives a larger relative negative potential energy (–71 kJ/mol, compared to –33 kJ/mol from empirical MD) for the ordered superstructure with respect to the ordered orthorhombic structure. This is because the empirical potential method does not explicitly consider electron interactions in the system but assigns fixed effective partial charges to each atom. While the absolute energy differences between structures with different carbonate orientations are different, the order of relative stabilities using the two methods agrees. In addition, all methods provide satisfactory estimates of unit-cell parameters. The deviation from experimental data is less
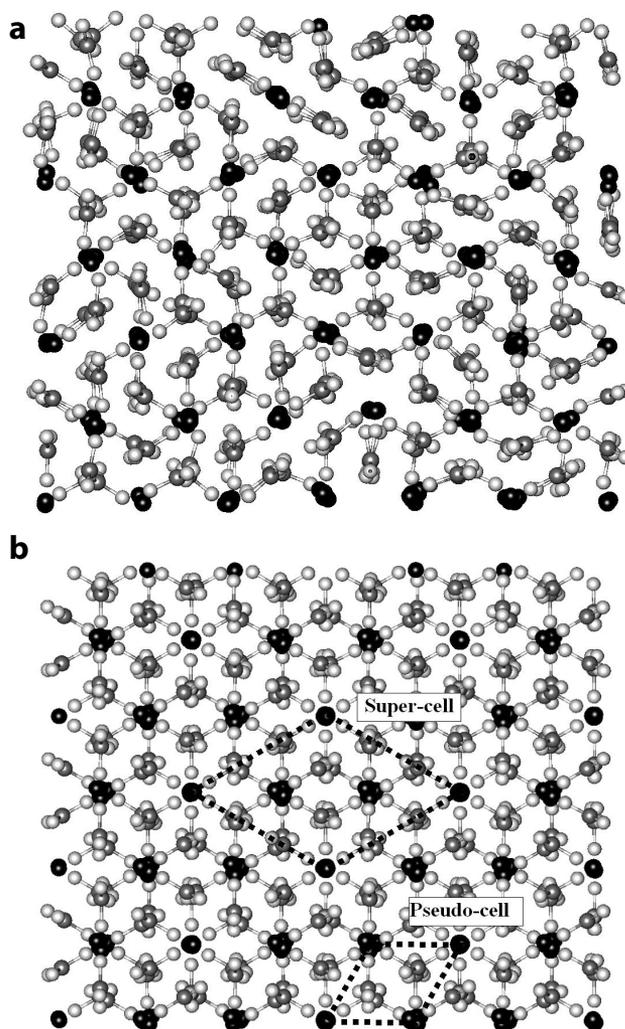
FIGURE 2. Snapshots of MD computational supercell structures from the temperature annealing MD simulation, projected onto (001) plane. The original computational supercell is hexagonal. The structure is plotted in a rectangular box for efficiency reasons, which is implemented in Gromacs package (van der Spoel et al. 2005). Scheme: light gray spheres are oxygen atoms, gray spheres are carbon atoms, and black spheres are calcium atoms. Image **a** is a snapshot at the end of the annealing cycle at 300 K, where CO$_3$ ions are disordered. Image **b** is a snapshot at the end of the annealing cycle at 1500 K, where they are ordered. The dashed lines highlight unit-cell dimensions for the pseudocell and supercell.

than 1% for the *c* dimension and less than 2% for *a* (*b*).

Fully disordered pseudocell and ordered supercell. A full description of the vaterite crystal structure requires both a pseudocell and a supercell. The former accounts for randomness and carbonate ion orientational disorder, and the latter captures long-range order of CO$_3$ ion orientation. A pseudocell found by Kamhi (1963) is a fully disordered structure. Each atom of the CO$_3$ ion is completely randomly distributed over three lattice sites. This structure is consistent with most spectroscopic studies and is supported by our temperature annealing MD simulation

TABLE 3. Energetics and unit-cell parameters of vaterite structures (CaCO$_3$)

Relative Energy (kJ/mol)*		a (nm)	b (nm)	c (nm)
$P1$ (Disordered) ($\alpha = \beta = 90°$, $\gamma = 120°$)				
MD	−22.7	0.7103	0.7103	2.5271
$P3_221$ hexagonal ($\alpha = \beta = 90°$, $\gamma = 120°$)				
GGA	−69.9	0.7214	0.7214	2.5401
MD	−33.3	0.7103	0.7103	2.5249
$P6_522$ hexagonal ($\alpha = \beta = 90°$, $\gamma = 120°$)				
GGA	−71.7	0.7290	0.7290	2.5302
MD	−33.3	0.7103	0.7103	2.5249
$P6_3/mmc$ hexagonal ($\alpha = \beta = 90°$, $\gamma = 120°$)				
Exp.†		0.716	0.716	2.547‡

Notes: The values from MD simulations are obtained by gradually decreasing the temperature from high temperature (500–1500 K) to 0 K. The values for the first-principles calculations are from optimized structures.
* For each method, the reference energy is based on vaterite with *Pbnm* structure.
† Kamhi 1963.
‡ A super-cell with $a = \sqrt{3} \times a'$ and $c = 3 \cdot c'$.

at annealing temperature 300 K. However, the small number of weak reflections (Kamhi 1963) and numerous diffuse streaks (Meyer 1969) in the X-ray diffraction patterns as well as the two independent site symmetries for CO$_3$ ions from the Raman spectra (Behrens et al. 1995) indicate the existence of some degree of long-range ordering and a superstructure. Although both single-crystal X-ray diffraction studies (Kamhi 1963; Meyer 1969) provide supercell dimensions, they do not supply any details for the superstructure such as atomic positions and symmetry, possibly because the vaterite samples are only partially ordered or contain a mixture of ordered and disordered domains. Stacking faults found by a single-crystal X-ray diffraction study (Meyer 1969) further complicate finding the true supercell.

The fully ordered superstructure found by our MD annealing simulation is hexagonal (Table 4). The unit-cell parameter a is 0.729 nm and c is 2.530 nm from the GGA-PAW calculation (Table 3). It has space group $P6_522$, or $P3_221$ if the coordinate tolerance is smaller (0.01 nm) when finding symmetry for the MD annealed structure (Fig. 2b). The unit cell of this hexagonal superstructure is rotated by 30° and $\sqrt{3}$ times longer in the a (b) dimension, and 3 times in the c dimension with respect to that of Kamhi's pseudocell structure (Kamhi 1963). Both unit cells are highlighted in Figure 2b. The new hexagonal supercell dimensions are consistent with the suggested supercell of earlier X-ray diffraction studies except for the c-axis dimension (Kamhi 1963; Meyer 1969). The supercell volume is 9 times that of the hexagonal pseudocell, with $Z = 18$. In this superstructure, the Ca atoms form a hexagonal lattice (Fig. 3). The planes of the CO$_3$ ions are parallel to the c axis and oriented with a 120° angle between them in an ordered fashion. Along the a or b axes, CO$_3$ ions in each row are oriented in the same direction. Each CO$_3$ ion is at the center of a prism of 6 Ca ions, all three oxygen atoms of CO$_3$ are pointing to the edges of the prism. Ca ions are coordinated by six O atoms at distances of about 0.23–0.25 nm and two more O atoms at 0.29–0.31 nm, consistent with the results of the disordered hexagonal structure (Kamhi 1963). The stacking sequence is ABC, resulting in a c dimension being tripled, instead of ABAB, doubled as suggested by Kamhi (1963) and Meyer (1969), which may originate from incomplete CO$_3$

ordering or stacking faults along c dimension in their samples. The structure found by our MD simulation is fully ordered with no stacking faults.

Disorder of freshly made vaterite

Comparing our calculated X-ray diffraction patterns with the experimental one by Han et al. (2006) (Fig. 4) indicates that the structure of freshly made vaterite by rapid gas-solution reaction at pH 7.9 is compatible with the disordered structure proposed by Kamhi (1963) and our model (Fig. 2a) with disordered CO$_3$ orientations. All calculated and experimental XRD patterns have very similar peak positions and shapes of the major reflections. The remaining differences are weak reflections with 2θ around 28.5, 34, and 38–39°. These peaks become more visible when CO$_3$ ions are more ordered. The calculated patterns from the disordered model (DSOD I) and the fully disordered hexagonal

TABLE 4. Vaterite structure from the first-principles calculation

Atomic positions	x/a	y/b	z/c
Ca1	0.991	0.011	0.083
Ca2	0.696	0.304	0.083
Ca3	0.339	0.661	0.083
C1	0.051	0.373	0.995
C2	0.000	0.309	0.667
O1	0.000	0.131	0.667
O2	0.990	0.391	0.622
O3	0.965	0.289	0.950
O4	0.226	0.551	0.997
O5	0.963	0.282	0.039

Notes: Cell parameters: $a = b = 0.7290$ nm, $c = 2.5302$ nm, $\alpha = \beta = 90°$, $\gamma = 120°$. Space group: $P6_522$ (no. 179).
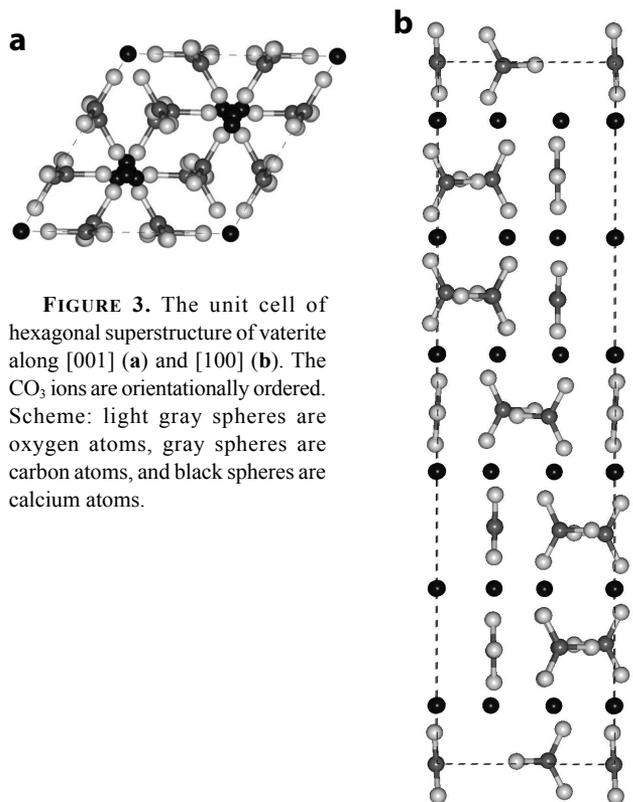
FIGURE 3. The unit cell of hexagonal superstructure of vaterite along [001] (**a**) and [100] (**b**). The CO$_3$ ions are orientationally ordered. Scheme: light gray spheres are oxygen atoms, gray spheres are carbon atoms, and black spheres are calcium atoms.

structure ($P6_3/mmc$) are very similar to the experimental one, with the absence of small reflection peaks in the experimental one in the 2θ range between reflections (113) and (116), and between (116) and (300), indicating that the sample has disordered CO_3 orientations. The patterns from the ordered models (OD and $P6_522$) have some additional weak reflections at 2θ ≈ 28.5, 34, and 38–39°. These reflections are much weaker in the intermediate disordered model (DSOD II, which is more ordered than DSOD I), which is consistent with the degree of CO_3 orientational order. Therefore, the peaks marked by stars in Figure 4 can serve as an order-disorder indicator.

Orientational order and disorder in vaterite

The vaterite structure can be considered as having hexagonal symmetry and a small basic pseudocell ($Z = 2$) with disordered CO_3 ions, which can be ordered in the a and b directions, resulting in two unique CO_3 ions. The lattice vectors a and b are turned by 30° from the original lattice vectors and √3 times longer than a and b of the hexagonal cell. There is ordering of the carbonate ions in the c direction, resulting in an ordered stacking (tripled) of the pseudocell by rotational symmetry operation along the c axis. The degree of ordering depends on sample preparation and thermal history. This view of the vaterite structure is supported by comparing calculated potential energies and volume changes of the ordered and disordered structures with available experimental data, e.g., enthalpy changes of transformations to calcite and changes in cell volumes of heat-treated samples.

Large variations in the measured enthalpies of transformation (from vaterite to calcite) of samples prepared at different conditions can be explained by different degrees of CO_3 orientational ordering in the structures. Based on our MD simulations, the calculated potential energy change is –10.6 kJ/mol from the disordered structure to the fully ordered one. Based on this estimate, a small fraction of ordering, for instance 10%, can reduce the potential energy by about 1.0 kJ/mol, which should be measurable by experimental methods. In fact, experimental results of the transition enthalpy (vaterite to calcite) vary from –3.4 ± 0.2 kJ/mol (Wolf et al. 2000) to –6.2 ± 1.7 kJ/mol (Plummer and Busenberg 1982). Moreover, a systematic thermochemical study (Turnbull 1973) shows that the enthalpy of transition can depend on sample-aging history. For freshly made vaterite, the enthalpy of transition to calcite is –4.3 kJ/mol, compared to –3.5 kJ/mol for an aged sample (2 h), suggesting a 0.9 kJ/mol enthalpy gain during aging. If this energy difference is entirely caused by ordering (assume the final product calcite is the same), based on our MD simulations, as little as 10% orientational carbonate ordering could account for such an enthalpy change. In the past, the enthalpy change with aging was related to surface and strain energies (Turnbull 1973). However, the energies were not estimated for vaterite. It is possible that CO_3 ordering occurs simultaneously with the decrease of surface area and crystal defects during sample preparation or aging and heat treatment. The contribution of orientational ordering to the enthalpy change is significant as demonstrated by our MD simulations, which has not been realized previously.

Orientational ordering of CO_3 ions in vaterite can also explain specific volume changes of the heat-treated samples at high temperatures. The specific volume of vaterite decreases by 0.64%
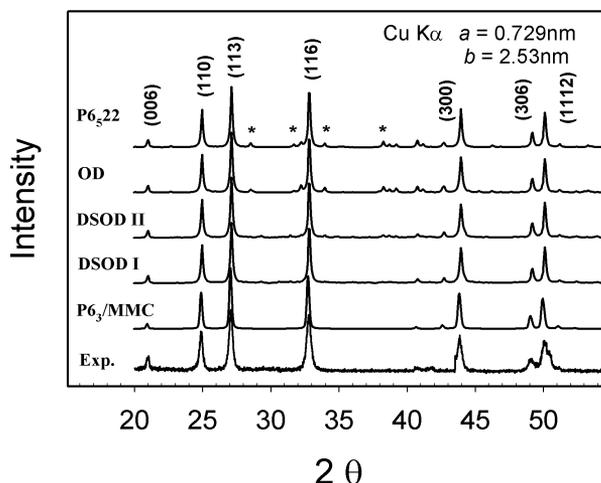
FIGURE 4. The calculated and experimentally observed X-ray diffraction patterns. Indexing is based on the hexagonal supercell with $a = 0.729$ nm and $c = 2.53$ nm from the first-principles optimized supercell. The patterns from bottom up are: experiment at pH 7.9 and room temperature (Exp.); completely disordered pseudocell ($P6_3/MMC$); disordered superstructure (DSOD I), which is annealed at 0 K with 300 K annealing temperature; more partially disordered superstructure (DSOD II), which is annealed at 0 K with 500 K annealing temperature; fully ordered annealed superstructure (OD), which is annealed at 0 K with 1500 K annealing temperature; and ordered supercell ($P6_522$).

for the sample heat-treated at 740 K with respect to the 470 K heat-treated one (Rao 1973). This volume contraction can be rationalized by internal structural changes of the thermally activated CO_3 orientational ordering during the heat treatment. Our temperature-annealing MD simulation results in a volume decrease of 0.47%, which is comparable to the experimental observation. There may be other causes for the decrease of the specific volume by heating such as healing of crystal defects and impurities, but the order-disorder contribution cannot be ignored.

CONCLUDING REMARKS

The experimental observations on both structure and energetics of inorganically formed vaterite in a laboratory setting are well explained by the order-disorder transition of CO_3 ions. It is not clear whether abiogenic and biogenic vaterite formation follows similar principles since the chemical composition of vaterite samples that are inorganically synthesized are much more pure than those of biogenic origin. It is well known that biomolecules, such as aspartic acid (Malkaj and Dalas 2004), can alter the stability of vaterite (Falini et al. 1998; Champ et al. 2000; Mann 2001; Malkaj and Dalas 2004; Wu et al. 2004). They must have a significant influence on order-disorder transitions and the stability of interfaces. Thus, it remains to be seen what effect the orientational ordering of CO_3 ions has on the stability, properties, and functionalities of biogenic vaterite.

REFERENCES CITED

Accelrys (1999) Forcefield-based simulations—Cerius² user manual. Accelrys Software Inc., San Diego.

Allen, M.P. and Tildesley, D.J. (1987) Computer simulation of liquids. Clarendon Press, Oxford.

Anderson, A. (1996) Group theoretical analysis of the ν1 (CO$_3^{2-}$) vibration in crystalline calcium carbonate. Spectroscopy Letters, 29, 819–825.

Ariani, A.P., Wittmann, K.J., and Franco, E. (1993) A comparative study of static bodies in mysid crustaceans: Evolutionary implications of crystallographic characteristics. Biological Bulletin, 185, 393–404.

Behrens, G., Kuhn, T.L., Ubic, R., and Heuer, H.A. (1995) Raman spectra of vateritic calcium carbonate. Spectroscopy Letters, 28, 983–995.

Blöchl, P.E. (1994) Projector augmented-wave method. Physical Review B, 50, 17953–17979.

Bradley, W.F., Graf, D.L., and Ro, R.S. (1966) The vaterite-type ABO$_3$ rare-earth borates. Acta Crystallographica, 20, 283.

Champ, S., Dickinson, J.A., Fallon, P.S., Heywood, B.R., and Mascal, M. (2000) Hydrogen-bonded molecular ribbons as templates for the synthesis of modified mineral phases. Angewandte Chemie International Edition, 39, 2716–2719.

Cygan, R.T. (2001) Molecular modeling in mineralogy and geochemistry. In R.T. Cygan and J.D. Kubicki, Eds., Molecular Modeling Theory and Applications in the Geosciences, 42, p. 1–35. Reviews in Mineralogy and Geochemistry, Mineralogical Society of America, Chantilly, Virginia.

Cygan, R.T., Liang, J.-J., and Kalinichev, A.G. (2004) Molecular models of hydroxide, oxyhydroxide, and clay phases and the development of a general force field. Journal of Physical Chemistry B, 108, 1255–1266.

de Leeuw, N.H. and Parker, S.C. (1998) Surface structure and morphology of calcium carbonate polymorphs calcite, aragonite, and vaterite: An atomistic approach. Journal of Physical Chemistry B, 102, 2914–2922.

Falini, G., Fermani, S., Gazzano, M., and Ripamonti, A. (1998) Oriented crystallization of vaterite in collagenous matrices. Chemistry: A European Journal, 4, 1048–1052.

Falini, G., Fermani, S., Vanzo, S., Miletic, M., and Zaffino, G. (2005) Influence on the formation of aragonite or vaterite by otolith macromolecules. European Journal of Inorganic Chemistry, 2005, 162–167.

Gabrielli, C., Jaouhari, R., Joiret, S., and Maurin, G. (2000) In situ Raman spectroscopy applied to electrochemical scaling. Determination of the structure of vaterite. Journal of Raman Spectroscopy, 31, 497–501.

Han, Y.S., Hadiko, G., Fuji, M., and Takahashi, M. (2006) Crystallization and transformation of vaterite at controlled pH. Journal of Crystal Growth, 289, 269–274.

Heywood, B.R. (1994) Biomineralization: New directions in crystal science. Microscopy Research and Technique, 27, 376–388.

Kalinichev, A.G., Wang, J., and Kirkpatrick, R.J. (2001) Structure of carbonate and bicarbonate aqueous solutions: Molecular simulation of ionic hydration and ion pairing. Eleventh Annual V.M. Goldschmidt Conference, abstract number 3293.

Kamhi, S. (1963) On the structure of vaterite CaCO$_3$. Acta Crystallographica, 16, 770–772.

Kanakis, J., Malkaj, P., Petroheilos, J., and Dalas, E. (2001) The crystallization of calcium carbonate on porcine and human cardiac valves and the antimineralization effect of sodium alginate. Journal of Crystal Growth, 223, 557–564.

Koneshan, S., Rasaiah, J.C., Lynden-Bell, R.M., and Lee, S.H. (1998) Solvent structure, dynamics, and ion mobility in aqueous solutions at 25 °C. Journal of Physical Chemistry B, 102, 4193–4204.

Kresse, G. and Furthmuller, J. (2004) Vienna Ab-initio Simulation Package. Universität Wein/University of Vienna.

Lippmann, F. (1973) Sedimentary Carbonate Materials. Springer, New York.

Malkaj, P. and Dalas, E. (2004) Calcium carbonate crystallization in the presence of aspartic acid. Crystal Growth and Design, 4, 721–723.

Mann, S. (2001) Biomineralization: Principles and Concepts in Bioinorganic Materials Chemistry. Oxford University Press, U.K.

Markgraf, S.A. and Reeder, R.J. (1985) High-temperature structure refinements of calcite and magnesite. American Mineralogist, 70, 590–600.

Medeiros, S.K., Albuquerque, E.L., Maia, F.F., Caetano, E.W.S., and Freire, V.N. (2007) First-principles calculations of structural, electronic, and optical absorption properties of CaCO$_3$ vaterite. Chemical Physics Letters, 435, 59–64.

Meyer, H.J. (1969) Struktur und fehlordnung des vaterits. Zeitschrift fur Kristallographie, 128, 183–212.

——— (1959) Versammlungsberichte. Angewandte Chemie, 71, 673–681.

Negro, A.D. and Ungaretti, L. (1971) Refinement of the crystal structure of aragonite. American Mineralogist, 56, 768–772.

Perdew, J.P. and Wang, Y. (1986) Accurate and simple density functional for the electronic exchange energy: Generalized gradient approximation. Physical Review B, 33, 8800–8802.

——— (1992) Accurate and simple analytic representation of the electron-gas correlation energy. Physical Review B, 45, 13244–13249.

Perdew, J.P., Chevary, J.A., Vosko, S.H., Jackson, K.A., Pederson, M.R., Singh, D.J., and Fiolhais, C. (1992) Atoms, molecules, solids, and surfaces: Applications of the generalized gradient approximation for exchange and correlation. Physical Review B, 46, 6671–6687.

Plummer, L.N. and Busenberg, E. (1982) The solubilities of calcite, aragonite and vaterite in CO$_2$-H$_2$O solutions between 0 and 90 °C, and an evaluation of the aqueous model for the system CaCO$_3$-CO$_2$-H$_2$O. Geochimica et Cosmochimica Acta, 46, 1011–1040.

Rao, M.S. (1973) Kinetics and mechanism of the transformation of vaterite to calcite. Bulletin of the Chemical Society of Japan, 46, 1414–1417.

Rodriguez-Navarro, C., Jimenez-Lopez, C., Rodriguez-Navarro, A., Gonzalez-Munoz, M.T., and Rodriguez-Gallego, M. (2007) Bacterially mediated mineralization of vaterite. Geochimica et Cosmochimica Acta, 71, 1197–1213.

Sato, M. and Matsuda, S. (1969) Structure of vaterite and infrared spectra. Zeitschrift fur Kristallographie, 129, 405–410.

Shen, Q., Wei, H., Zhou, Y., Huang, Y., Yang, H., Wang, D., and Xu, D. (2006) Properties of amorphous calcium carbonate and the template action of vaterite spheres. Journal of Physical Chemistry B, 110, 2994–3000.

Skinner, H.C.W. (2005) Biominerals. Mineralogical Magazine, 69, 621–641.

Turnbull, A.G. (1973) A thermochemical study of vaterite. Geochimica et Cosmochimica Acta, 37, 1593–1601.

van der Spoel, D. and others (2005) Gromacs user manual version 3.3, http://www.gromacs.org. University of Groningen, Netherlands.

Villiers, J.P.R. (1971) Crystal structures of aragonite, strontianite, and witherite. American Mineralogist, 56, 758–767.

Wang, J.W., Kalinichev, A.G., Kirkpatrick, R.J., and Hou, X.Q. (2001) Molecular modeling of the structure and energetics of hydrotalcite hydration. Chemistry of Materials, 13, 145–150.

Wang, J., Kalinichev, A.G., Amonette, J.E., and Kirkpatrick, R.J. (2003) Interlayer structure and dynamics of Cl-hydrotalcite: Far infrared spectroscopy and molecular dynamics modeling. American Mineralogist, 88, 398–409.

Wang, J., Kalinichev, A.G., and Kirkpatrick, R.J. (2006) Effects of substrate structure and composition on the structure, dynamics, and energetics of water at mineral surfaces: A molecular dynamics modeling study. Geochimica et Cosmochimica Acta, 70, 562–582.

Wolf, G., Königsberger, E., Schmidt, H.G., Königsberger, L.-C., and Gamsjäger, H. (2000) Thermodynamic aspects of the vaterite-calcite phase transition. Journal of Thermal Analysis and Calorimetry, 60, 463–472.

Wu, Q.-S., Sun, D.-M., Liu, H.-J., and Ding, Y.-P. (2004) Abnormal polymorph conversion of calcium carbonate and nano-self-assembly of vaterite by a supported liquid membrane system. Crystal Growth and Design, 4, 717–720.

Xiang, L., Wen, Y., Wang, Q., and Jin, Y. (2006) Synthesis of dispersive CaCO$_3$ in the presence of MgCl$_2$. Materials Chemistry and Physics, 98, 236–240.